

Strong Lyman- α emission in an overdense region at $z = 6.8$: a very large ($R \sim 3$ physical Mpc) ionized bubble in COSMOS?

Ryan Endsley ★ and Daniel P. Stark

Steward Observatory, University of Arizona, 933 N Cherry Ave, Tucson, AZ 85721, USA

Accepted 2022 February 22. Received 2022 February 18; in original form 2021 December 29

ABSTRACT

Our understanding of reionization has advanced considerably over the past decade, with several results now demonstrating that the intergalactic medium transitioned from substantially neutral at $z = 7$ to largely reionized at $z = 6$. However, little remains known about the sizes of ionized bubbles at $z \gtrsim 7$ as well as the galaxy overdensities which drive their growth. Fortunately, rest-ultraviolet (UV) spectroscopic observations offer a pathway towards characterizing these ionized bubbles thanks to the resonant nature of Lyman-alpha photons. In a previous work, we presented Ly α detections from three closely separated Lyman-break galaxies at $z \simeq 6.8$, suggesting the presence of a large ($R > 1$ physical Mpc) ionized bubble in the 1.5 deg² COSMOS field. Here, we present new deep Ly α spectra of 10 UV-bright ($M_{UV} \leq -20.4$) $z \simeq 6.6$ – 6.9 galaxies in the surrounding area, enabling us to better characterize this potential ionized bubble. We confidently detect ($S/N > 7$) Ly α emission at $z = 6.701$ – 6.882 in nine of ten observed galaxies, revealing that the large-scale volume spanned by these sources (characteristic radius $R = 3.2$ physical Mpc) traces a strong galaxy overdensity ($N/(N) \gtrsim 3$). Our data additionally confirm that the Ly α emission of UV-bright galaxies in this volume is significantly enhanced, with 40 per cent (4/10) showing strong Ly α emission (equivalent width > 25 Å) compared to the 8–9 per cent found on average at $z \sim 7$. The median Ly α equivalent width of our observed galaxies is also ≈ 2 times that typical at $z \sim 7$, consistent with expectations if a very large ($R \sim 3$ physical Mpc) ionized bubble is allowing the Ly α photons to cosmologically redshift far into the damping wing before encountering H I.

Key words: galaxies: high-redshift – dark ages, reionization, first stars.

1 INTRODUCTION

The epoch of reionization marks when radiation produced within the first galaxies ionized almost every hydrogen atom in the intergalactic medium (IGM). Over the past two decades, much effort has been devoted to understanding this connection between galaxy formation and the large-scale ionization state of the early Universe (Robertson 2021). One of the primary observational tools used to study the timeline of reionization is the Lyman-alpha emission line from high-redshift galaxies. Due to its resonant nature, Ly α is highly susceptible to scattering by H I, and thus will weaken considerably at epochs when the IGM is significantly neutral (e.g. Miralda-Escudé 1998; Haiman 2002; Mesinger, Haiman & Cen 2004; McQuinn et al. 2007). Many spectroscopic surveys have revealed that the fraction of typical ($M_{UV} \gtrsim -20$) star-forming galaxies showing strong Ly α falls abruptly at $z > 6$, suggesting that the IGM transitioned from largely ionized to significantly neutral between $z = 6$ and $z = 7$ (Fontana et al. 2010; Stark et al. 2010; Ono et al. 2012; Caruana et al. 2014; Pentericci et al. 2014, 2018; Schenker et al. 2014; Tilvi et al. 2014; Jung et al. 2017, 2020; Mason et al. 2018, 2019; Hoag et al. 2019; Fuller et al. 2020; Whitler et al. 2020). Such a reionization timeline is consistent with spectra of high-redshift quasars that indicate a low IGM neutral fraction at $z \simeq 6$ ($x_{HI} \lesssim 10$ per cent; McGreer, Mesinger

& D’Odorico 2015), yet a substantially neutral IGM at $z \simeq 7$ – 7.5 ($x_{HI} \sim 50$ per cent; Davies et al. 2018; Wang et al. 2020; Yang et al. 2020).

A key next step in studying reionization is understanding the growth of intergalactic H II regions. Due to spatial variations in structure formation, reionization is predicted to have been a patchy process where ionized bubbles covered certain portions of the early Universe while other volumes remained highly neutral (e.g. Ciardi et al. 2000; Miralda-Escudé, Haehnelt & Rees 2000). The first large ionized bubbles are expected to have formed around galaxy overdensities given the excess number of ionizing photons produced with them (e.g. Barkana & Loeb 2004; Furlanetto, Zaldarriaga & Hernquist 2004; Iliev et al. 2006; Castellano et al. 2016; Hutter et al. 2017; Kannan et al. 2021; Leonova et al. 2021; Garaldi et al. 2022). Over the coming decade, much effort is aimed at characterizing the size, spatial distribution, and associated overdensities of these ionized bubbles to provide detailed insight into how the IGM reionized.

One pathway towards identifying and mapping large ionized structures in the early IGM is using Ly α observations (e.g. McQuinn et al. 2007; Jensen et al. 2014; Castellano et al. 2018; Jung et al. 2020; Tilvi et al. 2020; Endsley et al. 2021b; Hu et al. 2021). When Ly α photons are emitted from galaxies within large ionized bubbles, they cosmologically redshift far into the damping wing before encountering neutral hydrogen, and hence transmit more efficiently through the IGM (Wyithe & Loeb 2005; Furlanetto, Zaldarriaga & Hernquist 2006; Weinberger et al. 2018; Mason & Gronke 2020; Park et al. 2021; Smith et al. 2021; Qin et al. 2022). Accordingly, a key indicator of a large ionized bubble is an enhanced Ly α equivalent

* E-mail: rendsley@email.arizona.edu

width (EW) distribution among galaxies within that volume. While it is straightforward to test if certain regions of the early Universe show enhanced Ly α , it has long been challenging to survey a big enough area on the sky to statistically sample large intergalactic H II regions. For reference, the largest ionized bubbles at $z = 7$ are predicted to span $\approx 15\text{--}30$ arcmin ($\approx 5\text{--}10$ physical Mpc) in diameter (Lin et al. 2016), suggesting that the identification of even just one of these bubbles may require Ly α observations covering multiple square degrees. A compounding challenge is that these wide areas must contain deep ($m \gtrsim 26$) near-infrared imaging since a rest-ultraviolet (UV) continuum measurement is necessary to determine the Ly α EW of individual galaxies.

In recent years, multiple ground-based imaging campaigns have begun reaching depths necessary to identify hundreds of $z \gtrsim 7$ Lyman-break galaxies across several square degrees (e.g. Bowler et al. 2014, 2020; Stefanon et al. 2019; Endsley et al. 2021a; Harikane et al. 2021). Spectroscopic follow-up of these sources is now underway and initial observations have already delivered a handful of Ly α detections out to $z = 7.2$ (Ono et al. 2012; Furusawa et al. 2016; Bouwens et al. 2021a; Endsley et al. 2021b). One notable outcome of these first results was the detection of Ly α from three closely separated UV-bright ($M_{\text{UV}} \leq -20.4$) galaxies at $z \simeq 6.8$ situated in the 1.5 deg² COSMOS field (Endsley et al. 2021b, hereafter E21b). Because Ly α is rarely seen from reionization-era galaxies, it was suggested that these sources may trace a large ionized bubble. The surrounding field also showed a high surface density of $z \simeq 6.8$ Lyman-break galaxies, hinting at the presence of a strong galaxy overdensity which would be expected to help generate a large intergalactic H II region.

In this paper, we present deep Ly α spectroscopy of 10 UV-bright ($M_{\text{UV}} \leq -20.4$) $z \simeq 6.8$ galaxies around the tentative ionized bubble identified in E21b. We detect Ly α emission from nine of 10 targeted galaxies (Section 3), confirming that the volume spanned by these sources (characteristic radius $R = 3.2$ physical Mpc) traces a strong overdensity ($N/\langle N \rangle \gtrsim 3$; Section 4.1). Our data also verify that the Ly α emission of UV-bright galaxies in this volume is significantly enhanced relative to average (Section 4.2), consistent with a picture wherein the surrounding IGM is highly reionized.

Throughout this paper, we quote magnitudes in the AB system (Oke & Gunn 1983), employ a Chabrier (2003) stellar initial mass function (IMF), and report 68 per cent confidence interval uncertainties. We also quote distances in physical units and adopt a flat Λ CDM cosmology with parameters $h = 0.7$, $\Omega_{\text{M}} = 0.3$, and $\Omega_{\Lambda} = 0.7$.

2 SAMPLE AND OBSERVATIONS

We are conducting a wide-area (7 deg²) spectroscopic survey targeting Ly α emission in Lyman-break selected galaxies at $z \sim 7$. One of the goals of this survey is to identify large ionized bubbles and quantify their local galaxy overdensities. In E21b, we described the first results from this campaign where we detected Ly α emission from three UV-bright systems in COSMOS with very similar redshifts ($z_{\text{Ly}\alpha} = 6.75\text{--}6.81$) and relatively small projected separations (< 5 arcmin). We suggested that these systems may trace a large ($R \gtrsim 2$ physical Mpc) ionized bubble formed by a local overdensity, as potentially evidenced by the high surface density of $z \simeq 6.8$ galaxy candidates in the surrounding region. To further characterize this field, we have since conducted ultra-deep (up to 25 h) Ly α spectroscopy of additional $z \simeq 7$ candidates in the surrounding 11×15 arcmin² area. With this ultra-deep data, we are able to measure Ly α fluxes and redshifts for more sources

and thus better quantify both the local Ly α EW distribution and galaxy overdensity. Below, we describe our target selection and the spectroscopic observations.

The wide-area (1.5 deg²) COSMOS field has been imaged with a large number of optical and near-infrared filters, enabling robust identification of the Lyman-alpha break at high redshifts. The Hyper Suprime-Cam (HSC) Subaru Strategic Program (HSCSSP; Aihara et al. 2018, 2019) provides optical imaging in the g , r , i , z , and y broad-band filters as well as nb816 and nb921 narrow-band filters. Additionally, COSMOS has been imaged in the HSC nb718, ib945, and nb973 filters with the Cosmic HyDRogen Reionization Unveiled with Subaru (CHORUS) survey (Inoue et al. 2020). In the near-infrared, the UltraVISTA survey (McCracken et al. 2012) has imaged COSMOS with the Y , J , H , and K_s broad-band filters of VISTA/VIRCam. We utilize PDR2 data of HSCSSP, PDR1 data of CHORUS, and DR4 data of UltraVISTA which are all calibrated to the *Gaia* astrometric reference frame.

Our selection of $z \simeq 7$ galaxies follows that described in Endsley et al. (2021a, hereafter E21a) and E21b. Briefly, we first extract sources from a χ^2 $yYJHK_s$ detection image (Szalay, Connolly & Szokoly 1999) and apply the colour cuts $z-y > 1.5$, $z-Y > 1.5$, $\text{nb921}-Y > 1.0$, and $y-Y < 0.4$. The enforcement of strong dropouts in z and nb921 identifies Lyman-alpha breaks at $z \gtrsim 6.6$ while the relatively flat $y-Y$ colour limits the selection window to $z \lesssim 6.9$. To minimize low-redshift contaminants, we also apply the cuts $S/N(g) < 2$ and $S/N(r) < 2$. Galactic brown dwarfs are removed from the sample by enforcing $Y-J < 0.45$ or ($J-H > 0$ and $J-K_s > 0$). To ensure each galaxy candidate is real, we require $S/N > 3$ detections in y , Y , and Y , as well as an $S/N > 5$ detection in at least one of those three bands. All HSC and VIRCam photometry are calculated in 1.2 arcsec diameter apertures with aperture corrections determined from the curve of growth of nearby stars.

We identify a total of 12 $z \simeq 6.6\text{--}6.9$ Lyman-break galaxies in an 11×15 arcmin² region of COSMOS surrounding the tentative ionized bubble reported in E21b. This 165 arcmin² area is fully contained within one of the ultra-deep UltraVISTA stripes, enabling us to select $z \simeq 6.6\text{--}6.9$ galaxies as faint as $J \sim 26$. The surface density of $z \simeq 6.6\text{--}6.9$ candidates in this region (0.0727 arcmin⁻²) is $2.85\times$ the average across the full 0.73 deg² area covered by the ultra-deep UltraVISTA stripes (0.0255 arcmin⁻²; see Fig. 1), perhaps indicating a large-scale (~ 5 physical Mpc) overdensity. We list the coordinates and photometric properties of all 12 systems in Table 1, where the three $z = 6.75\text{--}6.81$ Ly α emitters reported in E21b are COS-940214, COS-955126, and COS-1009842. All 12 galaxies have J -band magnitudes ranging from $m = 24.8$ to 26.3, corresponding to absolute UV magnitudes of $-22 \lesssim M_{\text{UV}} \lesssim -20.5$ at $z \simeq 6.8$. We measure the rest-UV slopes by fitting $f_{\lambda} \propto \lambda^{\beta}$ to the VIRCam $YJHK_s$ photometry, finding that our galaxies exhibit slopes spanning $-2.8 \leq \beta \leq -1.4$ consistent with values reported for larger samples of similarly bright $z \sim 7$ galaxies (e.g. Finkelstein et al. 2012; Bouwens et al. 2014; Bowler et al. 2017; Endsley et al. 2021a). As described above, we have assumed that apertures of 1.2 arcsec diameter (with point-source corrections) capture the large majority of flux coming from our $z \sim 7$ galaxies in the HSC and VIRCam imaging. This assumption is motivated by the expectation that $-22 \lesssim M_{\text{UV}} \lesssim -20.5$ galaxies at $z \sim 7$ will have half-light radii of $\approx 0.5\text{--}1$ kpc (i.e. $\approx 0.1\text{--}0.2$ arcsec; e.g. Shibuya, Ouchi & Harikane 2015; Curtis-Lake et al. 2016; Bowler et al. 2017), which are considerably smaller than our adopted 0.6 arcsec aperture radius. Indeed, if we adopt a larger aperture radius of 0.9 arcsec (e.g. Bowler et al. 2014), the derived near-IR flux densities of our galaxies typically increase by only 10 per cent (i.e. 0.1 mag).

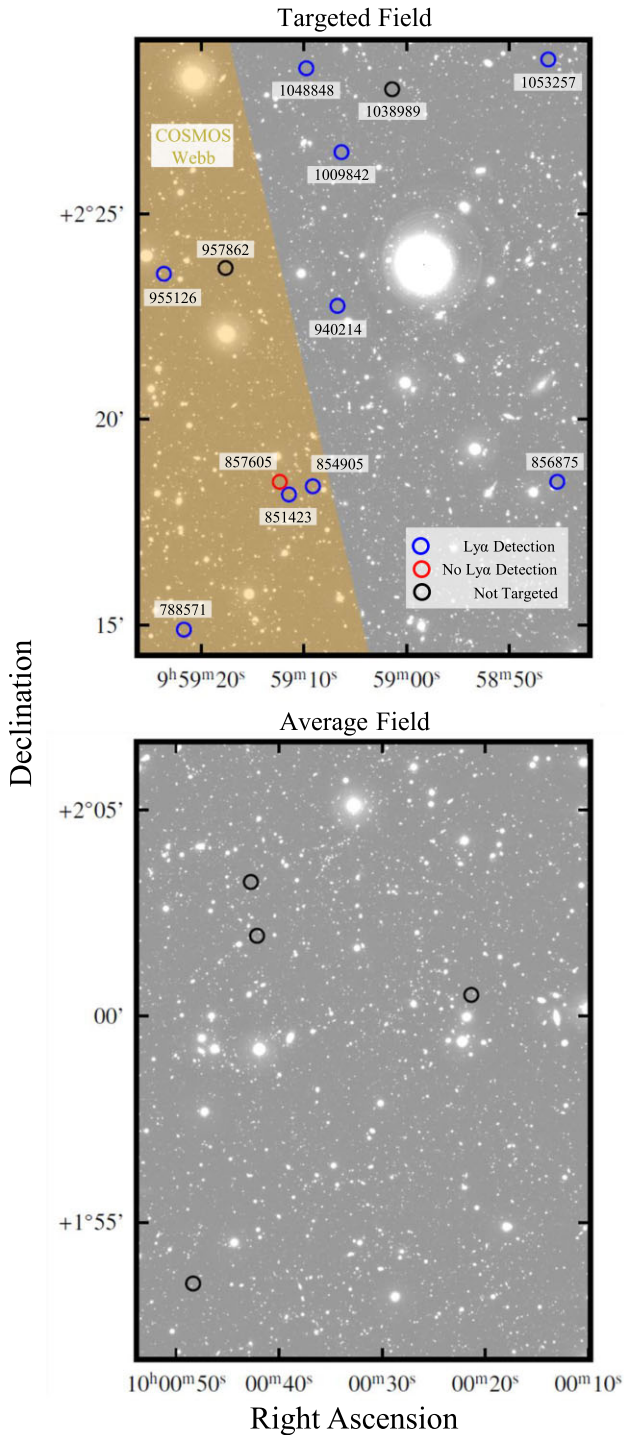


Figure 1. The top panel shows the 11×15 arcmin² area of COSMOS considered in this work. We mark the positions of $z \simeq 6.6$ – 6.9 Lyman-break sources with an MMT/Binospec Ly α detection (see Fig. 2) with blue circles. Those targeted with Binospec and not detected in Ly α are shown with red circles, while the remaining sources not targeted with Binospec are shown with black circles. The UltraVISTA J -band image is shown in the background with the footprint of the Cycle 1 *JWST* COSMOS-Webb survey (Kartaltepe et al. 2021) shown in orange. The bottom panel shows a sub-field of COSMOS with the same area, but with the average surface density of $z \simeq 6.6$ – 6.9 sources we identify across COSMOS. The surface density in our targeted field is $2.85\times$ this average value, suggesting the presence of a strong, large-scale (~ 5 physical Mpc) galaxy overdensity.

For the purpose of inferring stellar masses and ionizing properties, we also calculate the *Spitzer*/IRAC 3.6 and 4.5 μm photometry of our 12 $z \simeq 6.6$ – 6.9 systems. We use IRAC data from the SPLASH and SMUVS surveys (Steinhardt et al. 2014; Ashby et al. 2018) and co-add individual exposures using the MOPEX pipeline (Makovoz & Khan 2005) as described in E21a. Due to the broad point spread function of IRAC (FWHM ≈ 2 arcsec), we deconfuse the co-added images using morphological priors from the *HST*/F814W data available over COSMOS (Koekemoer et al. 2007; Massey et al. 2010) before calculating photometry in 2.8 arcsec diameter apertures (see E21b for further details). Upon visual inspection, we conclude the deconfusion residuals are acceptably smooth (see E21b) in all but one of the 12 identified $z \simeq 6.6$ – 6.9 systems in our targeted field. This galaxy, COS-957862, has a bright neighbouring source ≈ 1.5 arcsec to the East (i.e. within the IRAC FWHM) whose mid-infrared flux profile is not precisely matched by the F814W prior, resulting in a systematic pixel S/N offset within the aperture. Accordingly, we do not use the IRAC photometry for COS-957862. The [3.6]–[4.5] colours of the 11 remaining sources are all blue with several displaying [3.6]–[4.5] $\lesssim 1$ (see Table 1), suggesting generally strong [O III]+H β emission as expected among $z \sim 7$ galaxies (Smit et al. 2014, 2015; E21a). We come back to discuss the implied physical properties of these systems in Section 3.2.

We have thus far obtained Ly α spectra for 10 of the 12 $z \simeq 6.8$ galaxies described above (all but COS-957862 and COS-1038989). Spectroscopic observations were conducted using MMT/Binospec which is a wide-area (240 arcmin² field of view) multi-object optical spectrograph (Fabricant et al. 2019). We used the 600 l/mm grating for all observations, enabling sensitive spectroscopic coverage from ≈ 0.7 – 1.0 μm with moderately high resolution ($R \approx 4400$). Due to variable seeing and sky transparency between our Binospec exposures, we reduce each frame separately using the publicly available pipeline (Kansky et al. 2019) and then co-add the exposures following the weighting approach of Kriek et al. (2015). As described in E21b, we obtain 1D spectra using optimal extraction (Horne 1986) and determine the absolute flux calibration from the spectra of stars on each mask. We apply slit loss corrections using the size–luminosity relation of Curtis-Lake et al. (2012) which results in modest correction factors of 5–8 per cent for all galaxies in our sample given their expected small size (0.1–0.2 arcsec radii). These slit loss correction factors change very little (< 1 per cent) if we instead compute photometry in larger 1.8 arcsec diameter apertures. The total exposure time for each of the 10 targeted $z \simeq 6.6$ – 6.9 galaxies ranges from 18 900 to 91 900 s (5.2–25.5 h) with co-added average seeing between 0.9 and 1.0 arcsec (see Table 1).

3 RESULTS

In this section, we first present results from our MMT/Binospec Ly α spectra of UV-bright $z \simeq 6.6$ – 6.9 galaxies surrounding the tentative ionized bubble identified in E21b (Section 3.1). We then infer the physical properties of each galaxy by fitting their photometry with a photoionization model (Section 3.2), helping inform how efficiently these sources produce and emit Ly α photons.

3.1 MMT/Binospec spectra

We have targeted Ly α emission from 10 Lyman-break $z \simeq 6.6$ – 6.9 galaxies spanning an 11×15 arcmin² area around the potential ionized bubble reported in E21b (Fig. 1). Our ultra-deep MMT/Binospec spectra reveal an emission line detection in nine of 10 targeted sources (see Fig. 2). We interpret these emission lines

Table 1. Positions and photometric properties of the 12 $z \simeq 6.6\text{--}6.9$ galaxies identified across an 11×15 arcmin² region in COSMOS surrounding the tentative ionized bubble reported in E21b. For sources with a non-detection ($S/N < 1$) in one of the IRAC bands, we report the 2σ limiting colour. We do not report the IRAC colour for COS-957862 given the strong confusion from a bright neighbouring source. In the final column, we report the total MMT/Binospec exposure time and co-added average seeing for each targeted source. Neither COS-957862 nor COS-1038989 has yet been observed with Binospec.

Source ID	RA	Dec.	J	β	[3.6]–[4.5]	ib945– Y	Exp. time [s]	Avg. seeing [arcsec]
COS-788571	09:59:21.68	+02:14:53.02	$25.26^{+0.11}_{-0.10}$	-2.11 ± 0.55	$-0.92^{+0.21}_{-0.24}$	$0.17^{+0.23}_{-0.21}$	18900	0.92
COS-851423	09:59:11.46	+02:18:10.42	$25.90^{+0.22}_{-0.18}$	-2.64 ± 0.39	$-0.72^{+0.36}_{-0.48}$	$0.19^{+0.27}_{-0.25}$	91900	0.97
COS-854905	09:59:09.13	+02:18:22.38	$25.75^{+0.27}_{-0.22}$	-1.95 ± 0.24	$-0.44^{+0.31}_{-0.36}$	$0.20^{+0.34}_{-0.31}$	91900	0.97
COS-856875	09:58:45.34	+02:18:28.87	$25.63^{+0.29}_{-0.23}$	-2.06 ± 0.39	$-0.57^{+0.38}_{-0.44}$	$-0.96^{+0.26}_{-0.32}$	73100	0.98
COS-857605	09:59:12.35	+02:18:28.86	$25.76^{+0.23}_{-0.19}$	-1.38 ± 0.27	$-0.45^{+0.27}_{-0.34}$	$0.67^{+0.42}_{-0.35}$	65900	0.97
COS-940214	09:59:06.73	+02:22:45.93	$26.27^{+0.45}_{-0.31}$	-2.77 ± 0.54	< -1.26	$-0.87^{+0.36}_{-0.44}$	18900	0.92
COS-955126	09:59:23.62	+02:23:32.73	$25.38^{+0.24}_{-0.20}$	-2.44 ± 0.13	$-0.94^{+0.33}_{-0.44}$	$-0.16^{+0.24}_{-0.26}$	84700	0.95
COS-957862	09:59:17.62	+02:23:41.24	$25.62^{+0.17}_{-0.15}$	-2.12 ± 0.30	–	$1.38^{+1.24}_{-0.59}$	–	–
COS-1009842	09:59:06.33	+02:26:30.48	$26.22^{+0.26}_{-0.21}$	-2.59 ± 0.44	$-0.61^{+0.42}_{-0.53}$	$-0.74^{+0.28}_{-0.31}$	91900	0.97
COS-1038989	09:59:01.40	+02:28:02.28	$25.92^{+0.23}_{-0.19}$	-1.43 ± 0.30	$-0.97^{+0.56}_{-1.07}$	$0.27^{+0.53}_{-0.43}$	–	–
COS-1048848	09:59:09.76	+02:28:32.95	$26.09^{+0.27}_{-0.22}$	-2.43 ± 0.34	< -0.13	$0.59^{+0.55}_{-0.41}$	91900	0.97
COS-1053257	09:58:46.20	+02:28:45.76	$24.79^{+0.08}_{-0.07}$	-2.02 ± 0.20	$-0.33^{+0.33}_{-0.36}$	$0.70^{+0.23}_{-0.20}$	91900	0.97

as Ly α for the following reasons. First, the observed wavelength of each detected feature is consistent with a Ly α solution given the expected redshift range of our Lyman-break selection criteria ($z \simeq 6.6\text{--}6.9$). Secondly, none of the emission features appear to be an [O II] λ 3727,3729 doublet (i.e. two symmetric emission lines with an observed separation of ≈ 6.8 Å), and we moreover find that [O II] solutions are inconsistent with the photometric data of each source using the spectral energy distribution (SED) fitting procedure described in Section 3.2. We consider [O II] as the most likely alternative solution to Ly α since, if at low redshift, a Balmer break would likely be necessary to produce the very strong z and nb921 dropouts of each galaxy. Finally, we note that no other emission features are detected in these spectra, indicating that H β and [O III] λ 4959,5007 solutions are unlikely. The Ly α detections of four galaxies (COS-788571, COS-940214, COS-955126, and COS-1009842) were reported in E21b, though we have since obtained much deeper spectra (i.e. $3\text{--}5 \times$ longer integration) on the latter two galaxies.

The significance of each Ly α detection ranges from $7.5\text{--}24.9\sigma$ (see Table 2). These values are calculated by integrating the 1D line profile after masking regions contaminated by skylines, as determined from visual inspection to the 2D data (see Fig. 2). Because skylines appear to be obscuring significant portions of Ly α flux for some sources (e.g. COS-856875 and COS-940214), we determine the line properties (e.g. redshift and flux) of all galaxies by fitting their 1D spectra after masking the skyline-contaminated regions. We fit each spectra to a truncated Gaussian profile that accounts for varying degrees of line asymmetry seen in our sample (for example, compare the line shapes of COS-1009842 and COS-1048848 in Fig. 2):

$$F(\lambda) = \begin{cases} 0 & \text{for } \lambda < \lambda_{\text{cut}} \\ A e^{-(\lambda-\lambda_0)^2/2\sigma^2} + C & \text{for } \lambda \geq \lambda_{\text{cut}} \end{cases} \quad (1)$$

Here, A , λ_0 , and σ are the typical definitions of amplitude, peak wavelength, and standard deviation of a Gaussian profile, while C is the continuum flux density set equal to the value from the VIRCAM Y -band photometry. The value λ_{cut} defines the wavelength below which the Ly α optical depth rises sharply (due to absorption in either the circumgalactic or intergalactic medium), and is parametrized as $\lambda_{\text{cut}} \equiv \lambda_0 - k\sigma$ where we allow $0 \leq k \leq 3$ when fitting the data. A value of $k = 0$ yields a line with strong asymmetry while $k = 3$ results in

an almost perfectly symmetric profile. During each fit, we convolve the profile from equation (1) with the instrumental response ($R = 4400$) and use EMCEE (Foreman-Mackey et al. 2013) to determine confidence intervals on the four free parameters: A , λ_0 , σ , and k . The best-fitting Ly α profiles are shown in Fig. 2.

The peak wavelengths of the nine Ly α emission lines correspond to redshifts between $z_{\text{Ly}\alpha} = 6.701\text{--}6.882$ (see Table 2) as expected given our $z \simeq 6.6\text{--}6.9$ Lyman-break selection. After correcting for instrumental broadening, we find that the FWHM of each Ly α profile ranges between 149 and 542 km s^{−1}, with a median value of 272 km s^{−1} (Table 2). This is consistent with the median FWHM of ≈ 270 km s^{−1} measured from individual $z = 7\text{--}8$ Ly α spectra in Jung et al. (2020), and is slightly broader than the FWHM ≈ 220 km s^{−1} obtained from the stacked spectra of $z \sim 7$ Ly α emitters in Pentericci et al. (2018). The line fluxes of our Binospec-detected sample span $(3.7\text{--}17.3) \times 10^{-18}$ erg s^{−1} cm^{−2} (Table 2) where we have subtracted off the continuum with flux density assumed equal to that from the Y -band photometry. The rest-frame EWs derived from these line fluxes span $3.6\text{--}65.3$ Å (see Table 2), where four galaxies are found to exhibit strong Ly α emission ($\text{EW} > 25$ Å).

To check that the Ly α fluxes and EWs derived from our line-fitting procedure are reasonable, we also derive the EWs using an alternative approach that combines both the spectra and photometry. In much the same way that $z \sim 7\text{--}8$ [O III]+H β EWs can be inferred from IRAC colours, Ly α EWs can also be estimated from optical/near-infrared photometry if the redshift is known. At the redshifts of our galaxies ($z = 6.70\text{--}6.88$), the Ly α line falls within the HSC ib945 band and thus a blue ib945– Y colour will be seen in sources with sufficiently high Ly α EW. As a competing effect, the Ly α break also shifts into ib945 at $z > 6.65$ and thus will redden the ib945– Y colour to a larger degree at higher redshifts. Since we know the redshift from our Binospec spectra, we can calculate the rest-frame Ly α EW as

$$\text{EW}_{\text{ib945-}Y} = \frac{\text{BW}_{\text{ib945}} \times 10^{-0.4(\text{ib945-}Y)} - \int_{\lambda_{\text{Ly}\alpha}}^{\lambda_{\text{max}}} T_{\text{ib945}}(\lambda) d\lambda}{(1 + z_{\text{Ly}\alpha}) T_{\text{ib945}}(\lambda_{\text{Ly}\alpha})} \quad (2)$$

In this equation, BW_{ib945} is the bandwidth of the ib945 filter in Angstroms, $T_{\text{ib945}}(\lambda)$ is the filter throughput as a function of observed wavelength (normalized to a maximum value of unity), and λ_{max} is the maximum wavelength covered by ib945. The Ly α EWs (and corresponding fluxes) derived using this secondary approach are

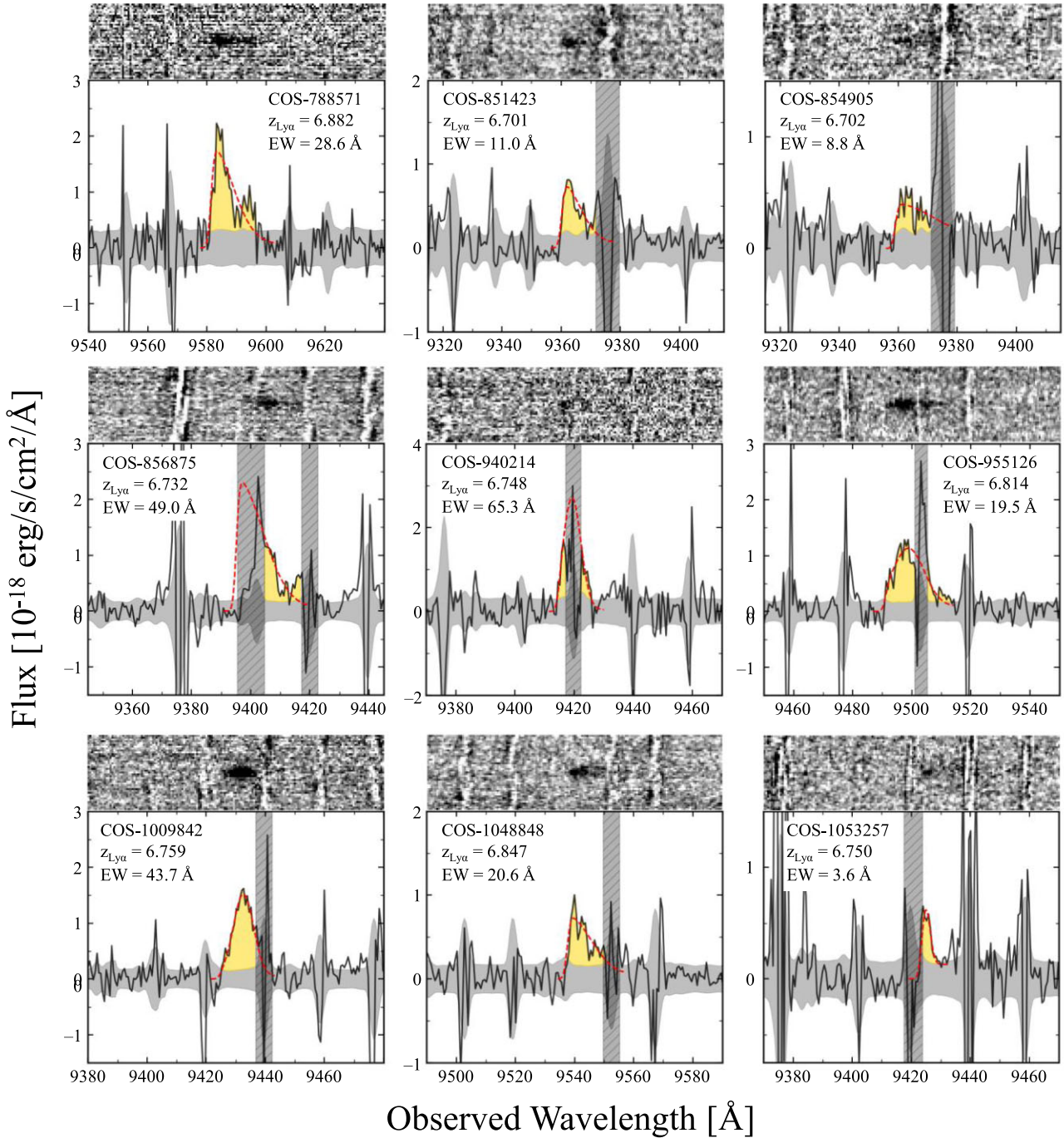


Figure 2. Lyman-alpha detections of nine of 12 $z \simeq 6.6$ – 6.9 Lyman-break galaxies identified across an 11×15 arcmin² region of COSMOS. 2D signal-to-noise maps are shown in the top sub-panels (black is positive) while the 1D extracted spectra are shown on the bottom with the 1σ error in grey. All detections have $S/N = 7.5$ – 24.9 where these values are calculated by integrating the 1D profiles after masking regions contaminated by skylines (shaded hatched regions in lower panels). The best-fitting truncated Gaussian profiles (see equation 1) are shown with dashed red lines and were fit excluding skyline-impacted regions.

listed in the last two columns of Table 2. These values all agree with those derived using the line-fitting procedure within uncertainties and no systematic offset is apparent between the two methods. We adopt the fluxes and EWs from the line-fitting approach as fiducial because this method most directly utilizes the Ly α spectra and results in more precise EW measurements for all sources.

We observe a range of Ly α profiles among our $z \simeq 6.8$ galaxies. Most sources show asymmetric Ly α lines (e.g. COS-788571, COS-851423, COS-854905, COS-955126, and COS-1048848; see Fig. 2),

as are commonly seen from galaxies due to resonant nature of Ly α emission (e.g. Kunth et al. 1998; Hu et al. 2004; Steidel et al. 2010). However, one of our galaxies (COS-1009842) appears to show a highly symmetric Ly α velocity profile with $k > 2$ at 92 per cent confidence (Fig. 2). Data of COS-1009842 indicate that this symmetric emission feature is unlikely to be a strong non-resonant optical line (i.e. H β , H α , [OIII] λ 4959, or [OIII] λ 5007) at lower redshift. Using the SED fitting procedure described in Section 3.2, we find that the photometry of COS-1009842 strongly

Table 2. Information on confident ($>7\sigma$) Ly α detections in our targeted $z \simeq 6.6$ – 6.9 galaxy sample. The line properties (redshift, FWHM, flux, and EW) are determined by fitting a truncated Gaussian (equation 1) to each observed 1D profile after masking skyline-contaminated regions of the spectra (see Fig. 2). In the final two columns, we report the EWs and fluxes derived by combining our measured Ly α redshifts with the ib945– Y colour of each source (see equation 2). No systematic offset is apparent between the two methods. We adopt the fluxes and EWs from the line-fitting approach as fiducial.

Source ID	$z_{\text{Ly}\alpha}$	S/N	FWHM [km s $^{-1}$]	Flux [10^{-18} erg s $^{-1}$ cm $^{-2}$]	EW [Å]	EW _{ib945–Y} [Å]	Flux _{ib945–Y} [10^{-18} erg s $^{-1}$ cm $^{-2}$]
COS-788571	6.882 $^{+0.001}_{-0.000}$	16.5	272 $^{+31}_{-29}$	15.1 $^{+1.2}_{-1.2}$	28.6 $^{+4.3}_{-3.6}$	34.4 \pm 8.4	18.2 \pm 4.9
COS-851423	6.701 $^{+0.001}_{-0.001}$	11.0	260 $^{+102}_{-57}$	5.2 $^{+1.1}_{-0.7}$	11.0 $^{+3.0}_{-2.1}$	2.6 \pm 9.9	1.2 \pm 4.8
COS-854905	6.702 $^{+0.002}_{-0.002}$	9.4	542 $^{+197}_{-170}$	4.8 $^{+1.4}_{-1.2}$	8.8 $^{+3.3}_{-2.4}$	2.1 \pm 12.0	1.2 \pm 6.7
COS-856875	6.732 $^{+0.002}_{-0.002}$	15.2	331 $^{+54}_{-49}$	18.5 $^{+5.1}_{-4.7}$	49.0 $^{+22.0}_{-15.0}$	67.4 \pm 24.6	25.6 \pm 11.5
COS-940214	6.748 $^{+0.001}_{-0.002}$	9.4	211 $^{+33}_{-27}$	17.3 $^{+3.9}_{-2.9}$	65.3 $^{+33.5}_{-18.6}$	64.4 \pm 31.6	17.5 \pm 10.5
COS-955126	6.814 $^{+0.000}_{-0.000}$	21.0	403 $^{+32}_{-32}$	13.0 $^{+0.9}_{-0.9}$	19.5 $^{+4.5}_{-3.2}$	38.8 \pm 13.2	25.8 \pm 10.1
COS-1009842	6.759 $^{+0.000}_{-0.000}$	24.9	258 $^{+23}_{-21}$	12.8 $^{+0.9}_{-0.8}$	43.7 $^{+12.8}_{-8.3}$	64.1 \pm 23.9	18.8 \pm 8.3
COS-1048848	6.847 $^{+0.001}_{-0.001}$	15.1	297 $^{+80}_{-54}$	6.6 $^{+1.1}_{-0.8}$	20.6 $^{+5.8}_{-4.1}$	13.4 \pm 10.3	4.3 \pm 3.5
COS-1053257	6.750 $^{+0.002}_{-0.002}$	7.5	149 $^{+56}_{-51}$	3.7 $^{+3.3}_{-1.8}$	3.6 $^{+3.3}_{-1.8}$	–3.4 \pm 4.2	–3.5 \pm 4.2

disfavours such low-redshift solutions (reduced $\chi^2 > 2.2$) while the Ly α solution well matches the data (reduced $\chi^2 = 0.6$). Furthermore, if this feature were H β , [O III] λ 4959, or [O III] λ 5007, at least one of the other two lines would lie in a skyline-free region of the spectrum where no emission is detected. We discuss what the symmetric Ly α velocity profile of COS-1009842 may imply for its ionizing efficiency and surrounding IGM in Section 4.

3.2 Photoionization modelling

A primary goal of this work is to test if the $z \simeq 6.6$ – 6.9 galaxies targeted in this paper have enhanced Ly α emission, as would be expected if they are situated in a large ionized bubble. Since the strength of Ly α could alternatively be boosted by properties internal to galaxies, we must first consider how the properties of these systems may impact their Ly α output. To this end, we infer the physical properties of the $z \simeq 6.6$ – 6.9 galaxies in our targeted field by fitting their photometry with the BEAGLE SED fitting tool (v0.20.4; Chevillard & Charlot 2016). We will compare the inferred properties of these systems to the larger ($N = 22$) Binospec-targeted sample of equally luminous ($M_{\text{UV}} \leq -20.4$) $z \simeq 6.6$ – 6.9 galaxies described in E21b.

BEAGLE utilizes the Gutkin, Charlot & Bruzual (2016) photoionization models of star-forming galaxies which include both stellar and nebular emission, computed by processing the latest version of the Bruzual & Charlot (2003) stellar population synthesis models through CLOUDY (Ferland et al. 2013). In BEAGLE, the posterior probability distributions of galaxy properties are derived from the input photometry using the Bayesian MULTINEST algorithm (Feroz & Hobson 2008; Feroz, Hobson & Bridges 2009). Our fitting procedure matches that described in E21b with the exception that we fold in the narrow/intermediate-band CHORUS data for sources lacking a spectroscopic detection, thereby providing more precise photometric redshifts (we also update the fits of the larger E21b sample with this new photometry). We employ a Chabrier (2003) IMF with mass limits of 0.1–300 M_{\odot} , adopt an SMC dust prescription (Pei 1992), and assume a delayed star formation history (SFR $\propto te^{-t/\tau}$) with an allowed superimposed recent (1–10 Myr) burst. Such bursts may have recently occurred within at least a subset of our UVB-bright $z \simeq 6.6$ – 6.9 systems showing very blue IRAC colours ([3.6]–[4.5] $\lesssim -1$) which are indicative of high-EW [O III]+H β emission (E21a). Because the transmission of Ly α photons is not a free parameter within BEAGLE, we remove Ly α emission from the model templates

and only fit data redward of the Lyman-alpha break for sources with a redshift measurement.

The resulting SED fits and inferred physical properties of each $z \simeq 6.6$ – 6.9 galaxy targeted in this paper are shown in Fig. 3 and Table 3, respectively. For completeness, we also include the two colour-selected sources that lie in the same small area as the other sources in this paper but have yet to be targeted with MMT/Binospec. All 12 galaxies have absolute UV magnitudes spanning $-22.0 \leq M_{\text{UV}} \leq -20.4$, corresponding to 0.9 – $4.0 \times$ the characteristic UV luminosity at $z \sim 7$ ($M_{\text{UV}}^* = -20.5$; Harikane et al. 2021). Among the 11 galaxies with robust IRAC measurements, the inferred stellar masses range from $\log_{10}(M_*/M_{\odot}) = 8.0$ to 9.1 with [O III]+H β EWs spanning 410–4040 Å (Table 3) as expected from their blue IRAC colours. Consistent with these large [O III]+H β EWs, we infer high specific star formation rates (sSFRs) ranging from 30 to 99 Gyr $^{-1}$ which are calculated using the average star formation rate over the past 10 Myr.

In the next section, we test for enhanced Ly α emission strengths among the 10 targeted galaxies that are the subject of this paper. To do so, we compare their median Ly α EW to that from the larger sample described in E21b. Our goal in this section is to determine whether we might expect to see substantial variation in the Ly α properties of the two samples based solely on differences in their physical properties. We first consider the dust content implied by the SED fitting results. Dust typically acts to absorb resonantly scattered Ly α photons, and not surprisingly observational measures of dust reddening are well known to be closely linked to the Ly α EW with redder galaxies typically showing weaker Ly α emission (e.g. Shapley et al. 2003; Pentericci et al. 2009; Kornei et al. 2010; Stark et al. 2010; Schenker et al. 2014; Hathi et al. 2016; Trainor et al. 2016; De Barros et al. 2017). BEAGLE quantifies the dust content in terms of the V-band dust optical depth parameter, τ_v , which can be converted into other extinction parameters as, e.g. $E(B - V) = 0.37\tau_v$ and $A_{1500} = 5.2\tau_v$ using the SMC extinction law adopted in this work. The SED fits suggest that the median dust content of the 10 galaxies targeted in this paper ($\tau_v = 0.02$) is essentially identical to that of the larger sample from E21b ($\tau_v = 0.03$). These values indicate minimal obscuration from dust, suggesting that both samples are likely to have ideal conditions to support the transmission of Ly α photons through the gas within the galaxies.

The production of Ly α can also vary considerably within the population. This is particularly important for reionization-era galaxies given the range of [O III]+H β EWs spanned by the population. The

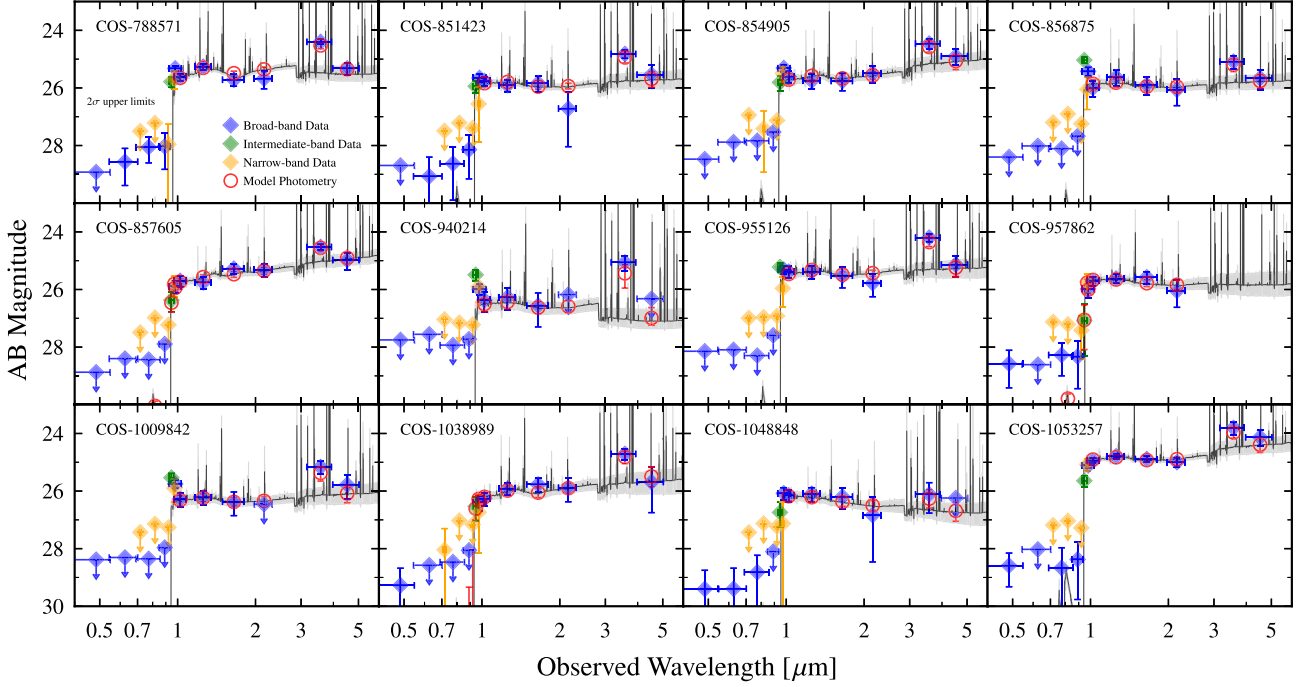


Figure 3. Optical through mid-infrared (0.3–5 μm) photometric SEDs of the 12 $z \approx 6.6\text{--}6.9$ galaxies in our targeted region of COSMOS. The blue, green, and orange diamonds show the broad-, intermediate-, and narrow-band data, respectively, with 2σ upper limits shown in cases of non-detections. The fitted median and 68 per cent confidence interval SEDs from BEAGLE are shown with the black line and grey shaded regions, respectively, in each panel. The associated model photometry is shown with red circles for fitted bands. We only fit data redward of the Ly α line for spectroscopically detected sources (see text).

Table 3. Inferred properties of the 12 $z \approx 6.6\text{--}6.9$ UV-bright galaxies identified within our targeted region of COSMOS. These properties were obtained using the BEAGLE SED fitting tool that adopts photoionization models of star-forming galaxies. The fiducial values and errors are determined by calculating the median and inner 68 per cent confidence interval values marginalized over the posterior probability distribution function output by BEAGLE. We report spectroscopic redshifts for sources with a Ly α detection and photometric redshifts for those without. In the final column, we report the estimated radius of the H II region generated by each individual source (see equation 3). We divide the table into those targeted with MMT/Binospec (top) and those not targeted (bottom). Due to the strong IRAC confusion for COS-957862 (see Section 2), we do not report inferred properties strongly dependent on rest-optical data for this source.

Source ID	Redshift	M_{UV}	τ_{v}	$\log_{10} M_{\star}$ [M_{\odot}]	sSFR [Gyr^{-1}]	[O III]+H β EW [\AA]	$\log_{10} \xi_{\text{ion}}$ [$\text{erg}^{-1} \text{Hz}$]	R_{HII} [pMpc]
Targeted with Binospec								
COS-788571	6.882	$-21.5^{+0.1}_{-0.1}$	$0.01^{+0.04}_{-0.01}$	$9.0^{+0.4}_{-0.3}$	44^{+49}_{-31}	4040^{+1930}_{-1730}	$26.32^{+0.18}_{-0.18}$	0.95
COS-851423	6.701	$-21.1^{+0.1}_{-0.1}$	$0.01^{+0.04}_{-0.01}$	$8.3^{+0.9}_{-0.3}$	85^{+107}_{-78}	1020^{+770}_{-500}	$25.72^{+0.14}_{-0.14}$	0.85
COS-854905	6.702	$-21.3^{+0.1}_{-0.1}$	$0.07^{+0.11}_{-0.06}$	$8.8^{+0.9}_{-0.5}$	67^{+110}_{-62}	670^{+530}_{-360}	$25.85^{+0.21}_{-0.19}$	0.90
COS-856875	6.732	$-21.0^{+0.2}_{-0.1}$	$0.02^{+0.06}_{-0.02}$	$8.5^{+0.7}_{-0.5}$	58^{+91}_{-51}	680^{+440}_{-340}	$25.68^{+0.16}_{-0.19}$	0.84
COS-857605	$6.73^{+0.05}_{-0.04}$	$-21.3^{+0.1}_{-0.1}$	$0.22^{+0.07}_{-0.08}$	$9.1^{+0.6}_{-0.5}$	30^{+69}_{-25}	470^{+370}_{-220}	$25.95^{+0.16}_{-0.23}$	0.91
COS-940214	6.748	$-20.4^{+0.2}_{-0.2}$	$0.01^{+0.04}_{-0.01}$	$8.0^{+0.4}_{-0.3}$	90^{+368}_{-62}	3170^{+1980}_{-2010}	$25.88^{+0.16}_{-0.18}$	0.69
COS-955126	6.814	$-21.5^{+0.1}_{-0.1}$	$0.01^{+0.05}_{-0.01}$	$8.5^{+0.8}_{-0.3}$	99^{+120}_{-90}	1500^{+930}_{-630}	$25.85^{+0.16}_{-0.12}$	0.96
COS-1009842	6.759	$-20.6^{+0.1}_{-0.1}$	$0.02^{+0.07}_{-0.02}$	$8.3^{+0.7}_{-0.4}$	69^{+111}_{-60}	900^{+720}_{-460}	$25.76^{+0.19}_{-0.16}$	0.73
COS-1048848	6.847	$-20.7^{+0.2}_{-0.1}$	$0.01^{+0.02}_{-0.01}$	$8.3^{+0.4}_{-0.4}$	45^{+65}_{-33}	410^{+520}_{-230}	$25.46^{+0.24}_{-0.26}$	0.74
COS-1053257	6.750	$-22.0^{+0.1}_{-0.1}$	$0.05^{+0.07}_{-0.04}$	$8.7^{+1.3}_{-0.4}$	98^{+132}_{-95}	510^{+410}_{-260}	$25.75^{+0.12}_{-0.20}$	1.13
Not targeted with Binospec								
COS-957862	$6.81^{+0.06}_{-0.06}$	$-21.2^{+0.1}_{-0.1}$	$0.02^{+0.06}_{-0.01}$	–	–	–	–	0.88
COS-1038989	$6.67^{+0.07}_{-0.06}$	$-20.8^{+0.1}_{-0.1}$	$0.11^{+0.12}_{-0.10}$	$8.5^{+0.7}_{-0.4}$	87^{+126}_{-74}	1230^{+1050}_{-680}	$26.07^{+0.18}_{-0.20}$	0.80

ionizing photon production rate (at fixed SFR) varies significantly with [O III]+H β EW (e.g. Chevillard et al. 2018; Tang et al. 2019), as expected given the close link between the latter quantity and the light-weighted age of the stellar population. Assuming case B recombination, variations in ionizing photon production lead to

variations in the production of Ly α . Such dispersion is observed at lower redshift, where the median Ly α EW is found to increase with [O III]+H β EW (e.g. Du et al. 2020; Tang et al. 2021). The median inferred [O III]+H β EW of the 10 galaxies observed in this work is 790 \AA (see Table 3), only 0.05 dex higher than that of the E21b

sample (710 Å). From the lower redshift studies (Tang et al. 2021), we expect this will cause a small ($\lesssim 0.05$ dex) increase in the Ly α EW.

We can also characterize potential variations in the Ly α production rate using the ionizing photon production efficiency (ξ_{ion}) implied by the BEAGLE models. Here, we define ξ_{ion} as the ratio of the production rate of Lyman-continuum photons (>13.6 eV) and the observed UV continuum luminosity at rest-frame 1500 Å. While other works adopt the ionizing photon production efficiency defined relative to the dust-corrected UV luminosity ($\xi_{\text{ion}}^{\text{HII}}$) or the intrinsic UV stellar continuum luminosity (ξ_{ion}^* , e.g. Matthee et al. 2017; Stark et al. 2017; Chevillard et al. 2018; Shivaei et al. 2018; Tang et al. 2019), we here use ξ_{ion} defined relative to the observed UV luminosity given that the Ly α EW is similarly defined. For reference, our inferred ξ_{ion} values are typically ≈ 0.05 and ≈ 0.10 dex larger than the inferred $\xi_{\text{ion}}^{\text{HII}}$ and ξ_{ion}^* values, respectively. Among the 10 galaxies observed in this work, we infer hydrogen ionizing photon production efficiencies of $\log_{10}[\xi_{\text{ion}}/(\text{erg}^{-1} \text{Hz})] = 25.46\text{--}26.32$ with a median $\log_{10}[\xi_{\text{ion}}/(\text{erg}^{-1} \text{Hz})] = 25.81$ (see Table 3). This median ξ_{ion} is essentially identical to that inferred among the E21b galaxies ($\log_{10}[\xi_{\text{ion}}/(\text{erg}^{-1} \text{Hz})] = 25.82$), suggesting that there are no significant differences in the typical ionizing photon production efficiency between the two samples. We note that these median inferred ξ_{ion} values are moderately (≈ 0.3 dex) larger than that expected from the $z \sim 2$ relation of Tang et al. (2019) connecting ionizing photon production efficiency and [O III] EW. None the less, if we instead adopted ξ_{ion} values using these low-redshift relations, we would still infer very little difference in the typical Ly α photon production rates of the two $z \sim 7$ samples ($\lesssim 0.03$ dex) given that their IRAC colors imply very similar median optical line EWs. Overall, we do not find any evidence that indicates that the 10 galaxies that form the basis of this paper would show significantly different Ly α properties than the larger sample observed in E21b. We will come back to this point in the next section.

4 ANALYSIS

We have two goals in this section. First, we utilize our Binospec redshift measurements to determine whether our targeted region of COSMOS traces a strong galaxy overdensity, as suggested by the high surface density of $z \simeq 6.6\text{--}6.9$ Lyman-break systems identified across the corresponding area (Section 4.1). Secondly, we explore whether our observed galaxies show significantly enhanced Ly α emission relative to the average at $z \simeq 7$, as would be expected if a very large ionized bubble has formed around these systems (Section 4.2).

4.1 A spectroscopic overdensity at $z = 6.8$

The high ($2.85\times$ average) surface density of $z \simeq 6.6\text{--}6.9$ Lyman-break galaxies across our targeted region of COSMOS implies a strong galaxy overdensity (see Fig. 1). Equipped with the line-of-sight position information from our Ly α detections, we can now spectroscopically constrain this overdensity. To do so, we compare the number of $M_{\text{UV}} \leq -21$ galaxies confirmed to lie in this region to the average number expected from $z \sim 7$ UV-luminosity functions derived from wide-area imaging (Bowler et al. 2017; Harikane et al. 2021). While we detect Ly α in systems as faint as $M_{\text{UV}} = -20.4$ (see Table 3), we restrict our attention to $M_{\text{UV}} \leq -21$ galaxies for this overdensity calculation to avoid luminosity regimes with low completeness. Due to the depth of the HSCSSP and UltraVISTA

imaging, the completeness of our $z \simeq 6.6\text{--}6.9$ Lyman-break selection declines sharply at $M_{\text{UV}} \gtrsim -21$ ($J \gtrsim 26$) to less than 10 per cent at $M_{\text{UV}} = -20.5$ (see fig. 2 of E21a).

Of the seven $M_{\text{UV}} \leq -21$ Lyman-break galaxies we targeted with Binospec, we have detected Ly α from $N = 6$ such systems. All six of these Ly α emitters were selected across an 11×15 arcmin² area and have redshifts between $z_{\text{Ly}\alpha} = 6.701\text{--}6.882$, indicating that they occupy a volume of $V = 3.5 \times 4.8 \times 8.3$ physical Mpc³ = 140 physical Mpc³. The average number of $M_{\text{UV}} \leq -21$ galaxies expected in this volume is $\langle N \rangle = 1.0^{+0.8}_{-0.5}$ from the Bowler et al. (2017) luminosity function (LF) and $\langle N \rangle = 2.0^{+0.9}_{-0.7}$ from the Harikane et al. (2021) LF. Because the results from these two LFs are consistent within 1σ uncertainties, we adopt the most conservative (i.e. largest) average number from the Harikane et al. (2021) LF as fiducial though include the Bowler et al. (2017) LF values in our reported errors. Our Binospec data therefore reveal a spectroscopic overdensity of at least $N/\langle N \rangle = 6.0/2.0^{+0.9}_{-1.5} = 3.0^{+9.0}_{-0.9}$ across the 140 physical Mpc³ volume spanned by our six confirmed $M_{\text{UV}} \leq -21$ Ly α emitters. We note that this quoted overdensity is a lower limit since we have not corrected N for either the spectroscopic completeness in detecting Ly α or the photometric completeness in selecting $M_{\text{UV}} \leq -21$ $z \simeq 6.8$ galaxies within our targeted volume. The calculated volume overdensity between $z = 6.70\text{--}6.88$ ($N/\langle N \rangle \gtrsim 3$) is consistent with the $2.85\times$ average surface density of $z \simeq 6.6\text{--}6.9$ Lyman-break galaxies identified across our targeted region of COSMOS.

With our Ly α detections, we can also measure the physical separations of our galaxies. Considering now all nine confirmed Ly α emitters in our sample, we find that our galaxies are separated by distances between $D = 0.20\text{--}8.4$ physical Mpc with a typical separation of 4.3 physical Mpc. Here, we are ignoring the line-of-sight position uncertainty due to differences in peculiar motions and Ly α velocity offsets of our galaxies. For reference, a combined 200 km s^{-1} difference between two galaxies at $z = 6.8$ would yield a derived line-of-sight separation of 0.2 physical Mpc, much smaller than the typical separation of our galaxies. The two Ly α emitters with the largest distance from one another are COS-851423 ($z_{\text{Ly}\alpha} = 6.701$) and COS-788571 ($z_{\text{Ly}\alpha} = 6.882$), where their separation is mainly along the line-of-sight direction (8.3 physical Mpc). Accounting for line-of-sight position uncertainties due to peculiar motions (~ 0.2 physical Mpc) translates to a small (~ 3 per cent) systematic error in our estimated 140 physical Mpc³ volume above. The two most closely separated galaxies in our sample (COS-851423 and COS-854905) have essentially equal Ly α redshifts ($z = 6.701\text{--}6.702$) and are located only 37 arcsec apart on the sky, translating to a physical separation of $D = 200$ kpc. Notably, there are two other galaxy pairs in our Binospec-detected sample with fairly small physical separations ($D < 2$ Mpc). COS-940214 and COS-1009842 are located 1.3 physical Mpc apart while COS-1009842 and COS-1053257 are separated by 1.8 physical Mpc.

Given the relatively small physical separation ($D \lesssim 1$ Mpc) between some of our galaxies, we consider whether these individual sources could generate ionized bubbles of sufficient size to have overlapped. We approximate the radius of an H II region, R_{HII} , generated by a single $z \sim 7$ galaxy using the equation (e.g. Haiman & Loeb 1997)

$$\frac{dR_{\text{HII}}}{dt} = \frac{\langle \xi_{\text{ion}} \rangle \langle f_{\text{esc}} \rangle L_{\text{UV4pt}}}{4\pi R_{\text{HII}}^2 \bar{n}_{\text{H}}(z)} + R_{\text{HII}} H(z) - R_{\text{HII}} \alpha_B \bar{n}_{\text{H}}(z) \frac{C_{\text{HI}}}{3}. \quad (3)$$

In this equation, the first and second terms on the right account for bubble growth due to photoionization and the Hubble flow, respectively, while the third term accounts for recombinations in

the IGM. The terms $\bar{n}_{\text{HI}}(z)$ and $H(z)$ are, respectively, the average H I density and *Hubble* parameter at the redshift corresponding to the associated time-step. For the case B recombination coefficient, we assume a temperature of 10^4 K yielding $\alpha_B = 2.59 \times 10^{-13} \text{ cm}^3 \text{ s}^{-1}$ (Osterbrock & Ferland 2006) and we set the IGM H I clumping factor, C_{HI} , to a fixed value of 3 (see e.g. Robertson et al. 2013). Finally, $\langle \xi_{\text{ion}} \rangle$ and $\langle f_{\text{esc}} \rangle$ are the average ionizing photon production efficiency and escape fraction, respectively, during the lifetime of the emitting galaxy.

The inferred ages of our galaxies are largely determined by their IRAC colours which probe the strength of [O III]+H β emission relative to the underlying optical continuum. A subset of our galaxies show IRAC colours suggesting extremely strong [O III]+H β emission ($\text{EW} \geq 1500 \text{ \AA}$; see Table 3), thereby implying very young ages ($t \lesssim 10$ Myr) assuming a constant star formation history. In these systems, it is possible that an older stellar population is being outshined by a recent strong upturn of star formation activity, limiting our knowledge of the true duration of ionizing photon production in these systems (e.g. Tang, Stark & Ellis 2022). We thus adopt a single time-scale for star formation (and hence ionizing photon production) for all our galaxies which is estimated from the typical $z \simeq 7$ [O III]+H β EW of 760 \AA (E21a). This EW corresponds to a galaxy age of approximately 200 Myr assuming a constant star formation history with 0.2 solar metallicity, ionization parameter of $\log U = -2.5$, and dust-to-metal mass ratio $\xi_d = 0.3$ using the Gutkin et al. (2016) photoionization models of star-forming galaxies. Over this 200 Myr age, we adopt a time-averaged ionizing photon production efficiency and escape fraction of $\langle \xi_{\text{ion}} \rangle = 10^{25.8} \text{ erg}^{-1} \text{ Hz}$ (Stark et al. 2017; De Barros et al. 2019; E21b) and $\langle f_{\text{esc}} \rangle = 0.2$ (e.g. Robertson et al. 2013), respectively. As discussed in Section 3.2, low-redshift observations (Tang et al. 2019) predict $\approx 2 \times$ lower ionizing photon production efficiencies for our galaxies relative to that inferred from BEAGLE. However, adopting these lower ξ_{ion} values would only change our estimated bubble sizes by a modest ≈ 0.1 dex (i.e. ≈ 25 per cent). A factor of 2 change in our assumed f_{esc} would have an equally modest effect.

Based on the assumptions above, it is plausible that each of our UV-bright ($M_{\text{UV}} \leq -20.4$) $z \simeq 6.6$ – 6.9 galaxies reside in ionized bubbles with radii of $R = 0.69$ – 1.13 physical Mpc (see Table 3). If these size estimates are correct, all three of the closely separated ($D < 2$ physical Mpc) galaxy pairs in our sample (COS-851423 + COS-854905, COS-940214 + COS-1009842, and COS-1009842 + COS-1053257) will each occupy a single ionized bubble. This is likely a conservative conclusion given that we are ignoring the ionizing photon contribution from fainter ($M_{\text{UV}} \gtrsim -20$) sources within our targeted ground-based imaging field. The spectroscopic overdensity we have confirmed exists in our observed $z \simeq 6.8$ volume ($N/(N) \gtrsim 3$) suggests that such faint sources are abundant and hence perhaps contribute substantially to the local ionizing photon budget. If this is indeed the case, we are likely significantly underestimating the sizes of ionized bubbles around each of our identified UV-bright ($M_{\text{UV}} \leq -20.4$) galaxies, possibly to the extent that all their surrounding bubbles have overlapped. We consider whether the entire 140 physical Mpc³ volume spanned by our confirmed Ly α emitters could plausibly have been reionized by considering ionizing photon contribution from all $M_{\text{UV}} \leq -17$ galaxies in this region (see also Rodríguez Espinosa, Mas-Hesse & Calvi 2021). Here, we assume an overdensity of $N/(N) = 3$ and apply equation (3) with fixed values of $\langle \xi_{\text{ion}} \rangle = 10^{25.8} \text{ erg}^{-1} \text{ Hz}$ and age = 200 Myr. With these assumptions, we find that our observed overdense field could have been reionized by $M_{\text{UV}} \leq -17$ galaxies if their escape fractions are at least $\langle f_{\text{esc}} \rangle \geq 6$ per cent. Such modest escape fractions are consistent with those

measured from star-forming galaxies at $z \lesssim 3$ (e.g. Shapley et al. 2016; Izotov et al. 2016a,b, 2018a,b; Steidel et al. 2018; Vanzella et al. 2018; Fletcher et al. 2019; Pahl et al. 2021; Begley et al. 2022; Flury et al. 2022; Saxena et al. 2022), implying that our targeted region could plausibly be fully reionized. In this scenario, the 140 physical Mpc³ volume spanned by our confirmed Ly α emitters translates to a characteristic bubble radius of $R = (3V/4\pi)^{1/3} = 3.2$ physical Mpc.

4.2 Enhanced Ly α emission: a very large ionized bubble?

If our observed galaxies in fact occupy a single very large ($R = 3.2$ physical Mpc) ionized bubble, we would expect their Ly α photons to cosmologically redshift far into the damping wing before encountering intergalactic H I and thus transmit efficiently through the IGM. Below, we explicitly calculate this transmission efficiency and compare to the case when Ly α is emitted within a more moderate-sized ($R = 0.7$ – 1.25 physical Mpc) bubble that might be generated by an individual UV-bright ($-20.5 \leq M_{\text{UV}} \leq -22.5$) $z = 7$ galaxy (see equation 3). We adopt the damping wing transmission calculations of Miralda-Escudé (1998) and assume that the IGM within an ionized bubble has a residual H I fraction of $x_{\text{HI}} \lesssim 10^{-5}$ (Mason & Gronke 2020) while the IGM outside the bubble is fully neutral. We also assume a Ly α velocity offset range of 100–500 km s⁻¹ as expected for UV-bright $z \simeq 7$ systems (Maiolino et al. 2015; Willott et al. 2015; Pentericci et al. 2016; Stark et al. 2017; Mason et al. 2018; Hashimoto et al. 2019; Endsley et al. 2022). With these assumptions, we find that a high fraction (≈ 80 per cent) of Ly α photons would transmit through the IGM when emitted from a UV-bright $z = 7$ galaxy at the centre of a very large ($R = 3.2$ physical Mpc) ionized bubble. When Ly α photons are instead emitted from the centre of a more moderate-sized ($R = 0.7$ – 1.25 physical Mpc) bubble, the expected IGM transmission fraction drops significantly to $T \approx 30$ – 60 per cent, a factor of 1.3 – $2.6 \times$ lower.

We now explore whether our Binospec data support the presence of a very large ($R \sim 3$ physical Mpc) ionized bubble within our observed overdense volume by testing for enhanced Ly α emission among our sample. To do so, we first compare the median Ly α EW from the 10 UV-bright ($M_{\text{UV}} \leq -20.4$) galaxies observed in this work to that from a larger ($N = 22$) Binospec-targeted sample of equally luminous $z \simeq 6.8$ galaxies described in E21b. This E21b sample was assembled by applying the same Lyman-break selection technique (see Section 2) across a much wider area (3 deg^2 versus 0.05 deg^2), thereby providing a more cosmologically averaged census of Ly α visibility among UV-bright $z \simeq 7$ galaxies. As described in E21b, the median Ly α EW of this wider-area sample was inferred to be $10 \pm 3 \text{ \AA}$. In contrast, the 10 UV-bright galaxies observed in this work reveal a median Ly α EW of 20 \AA (see Table 2). This suggests that the Ly α emission of UV-bright ($M_{\text{UV}} \leq -20.4$) $z \simeq 6.8$ galaxies within our targeted overdense field is enhanced by a factor of $2.0^{+0.9}_{-0.5}$ relative to average. As discussed below, this boost in the median Ly α EW is unlikely to be driven by abnormal galaxy properties among our sample.

To further test for enhanced Ly α visibility within our targeted overdense volume, we now compare the fraction of our galaxies showing strong ($\text{EW} > 25 \text{ \AA}$) Ly α emission against that from other UV-bright $z \sim 7$ galaxy samples in the literature. Using spectroscopic observations covering multiple deep *HST* fields, Pentericci et al. (2018) find a strong Ly α emitter fraction of 9^{+7}_{-4} per cent among $M_{\text{UV}} < -20.25$ $z \sim 7$ galaxies, in agreement with the value of 8^{+5}_{-4} per cent from Schenker et al. (2014). In contrast, 40 per cent (4/10) of the similarly luminous ($M_{\text{UV}} \leq -20.4$) galaxies observed

in this work show Ly α EW $> 25 \text{ \AA}$ (see Table 2). This factor of 4–5 increase in the strong Ly α -emitter fraction is expected if the EWs of our galaxies are typically boosted by a factor of approximately 2, at least assuming the average UV-bright ($M_{\text{UV}} \leq -20.4$) $z \simeq 7$ Ly α EW distribution inferred in E21b. The E21b lognormal Ly α EW distribution (approximate median EW of 10 \AA with 0.35 dex scatter) implies a typical strong Ly α -emitter fraction of ≈ 12 per cent, consistent with the findings of Pentericci et al. (2018) and Schenker et al. (2014). If we boost the median EW of this distribution by a factor of 2 (to 20 \AA) at fixed scatter, the strong Ly α -emitter fraction rises to ≈ 40 per cent as seen among our observed sample.

The two metrics of Ly α visibility described above (the median EW and the strong Ly α -emitter fraction) both indicate that our observed UV-bright ($M_{\text{UV}} \leq -20.4$) $z \simeq 6.8$ galaxies show significantly enhanced Ly α emission. As motivated in Section 3.2, the factor of $2.0_{-0.5}^{+0.9}$ enhancement in median Ly α EW among our galaxies relative to the wider-area E21b sample is unlikely to be driven by differences in galaxy physical conditions. These two samples have nearly equal median hydrogen ionizing photon production efficiencies ($\log_{10}[\xi_{\text{ion}}/(\text{erg}^{-1} \text{ Hz})] = 25.81$ versus 25.82), V-band dust optical depths ($\tau_v = 0.02$ versus 0.03), and [O III]+H β EWs (790 versus 710 \AA), implying a very similar efficiency of Ly α photon production and escape (Section 3.2). The $\approx 2 \times$ increased median Ly α EW of our observed galaxies may instead indicate that the large-scale volume ($140 \text{ physical Mpc}^3$) hosting these systems is highly reionized. As detailed above, it is feasible that the Ly α damping wing transmission of our galaxies would be twice that typical of UV-bright $z \sim 7$ systems if our targeted field contains a single very large ($R = 3.2 \text{ physical Mpc}$) ionized bubble. The presence of such a large bubble around our galaxies is qualitatively consistent with expectations given the strong galaxy overdensity ($N(N) \gtrsim 3$) we have confirmed exists in our observed volume (e.g. Barkana & Loeb 2004; Wyithe & Loeb 2005; Hutter et al. 2017; Garaldi et al. 2022; Qin et al. 2022).

The Ly α profiles of our galaxies offer another way to explore whether our targeted $z \simeq 6.8$ volume may contain a very large ($R \gtrsim 3 \text{ physical Mpc}$) ionized bubble. Prior to the completion of reionization, Ly α photons emitted blueward of systemic velocity will often be completely undetectable given their extremely high optical depth to intergalactic H I. Hence, blue-sided Ly α can only become significantly transparent at $z \gtrsim 7$ if the emitting galaxy resides in a large ionized bubble, enabling the photons to cosmologically redshift into the red part of the damping wing before reaching the edge of the bubble (e.g. Matthee et al. 2018; Mason & Gronke 2020; Gronke et al. 2021; Meyer et al. 2021; Smith et al. 2021). Below, we search for evidence of blue-sided Ly α emission from our Binospec-detected galaxies. We note that, even if our galaxies do occupy a large bubble, we should not necessarily expect them to show blue-sided Ly α emission since these photons can also be heavily attenuated by H I within the circumgalactic medium (CGM; e.g. Henry et al. 2015; Gazagnes et al. 2020). None the less, the detection of blue-sided Ly α emission from even just one of our galaxies would necessitate the presence of a large H II region within our targeted volume.

We presented the Ly α line profiles of our sample in Section 3.1. One of our galaxies (COS-1009842, see Section 3.1 and Fig. 2) was shown to exhibit a highly symmetric Ly α profile. As we motivate above, this may provide additional evidence for a large ionized bubble in our observed field. Because resonant interactions with neutral hydrogen will distort Ly α profiles, one interpretation of the symmetry is that the observed profile closely matches the intrinsic profile, with the observed peak tracing systemic velocity

(see e.g. the $z \approx 2$ galaxy XLS-20 in Naidu et al. 2022 for one such known example). In this scenario, we are detecting Ly α photons emitted both blueward and redward of systemic. The implied scarcity of resonant interactions would necessitate that the observed Ly α photons are escaping COS-1009842 through a highly ionized channel in the interstellar medium (ISM) and CGM, thus indicating a non-unity H I covering fraction and hence efficient ionizing photon escape from this system (e.g. Izotov et al. 2018a; Jaskot et al. 2019; Gazagnes et al. 2020; Naidu et al. 2022). Furthermore, because Ly α photons blueward of systemic velocity are extremely sensitive to neutral hydrogen, the observed symmetry would require a very large, highly ionized bubble around COS-1009842. To preserve the line symmetry to within ≈ 10 per cent across the width of the line (FWHM = 260 km s^{-1} ; see Table 2), we estimate that the Ly α photons must travel through an ionized path-length of at least ≈ 3 physical Mpc along the line of sight (see fig. 1 of Mason & Gronke 2020). However, this is not the only potential interpretation of the symmetric Ly α profile observed from COS-1009842. We cannot currently rule out the possibility that this source possesses abnormal outflow properties that would lead to a symmetric Ly α profile with a peak centred substantially redward of systemic velocity. Ultimately, a systemic redshift measurement from e.g. [O III] $\lambda 5007$ or [C II] $\lambda 158 \mu\text{m}$ will be required to determine if the Ly α profile of COS-1009842 implies efficient ionizing photon escape as well a surrounding very large ($R \gtrsim 3 \text{ physical Mpc}$) ionized bubble.

Ly α spectra of fainter ($M_{\text{UV}} > -20$) $z \simeq 6.8$ sources within our observed field can further help characterize the surrounding IGM ionization state. Because fainter $z \sim 7$ galaxies are expected to possess lower Ly α velocity offsets (Erb et al. 2014; Stark et al. 2017; Mason et al. 2018), their photons are intrinsically closer to line centre and are thus more susceptible to intergalactic H I if emitted within relatively small ionized bubbles. Accordingly, if our targeted region of COSMOS indeed contains a very large ($R = 3.2 \text{ physical Mpc}$) bubble, the Ly α EW enhancement among the fainter population should exceed the factor of ≈ 2 increase we find among our UV-bright ($M_{\text{UV}} \leq -20.4$) sample. To quantify this more directly, we consider the scenario that a typical $M_{\text{UV}} = -19$ galaxy at $z = 7$ has a Ly α velocity offset of 100 km s^{-1} (Mason et al. 2018) and lies at the centre of a small ionized bubble with $R = 0.4 \text{ physical Mpc}$ (equation 3). The expected Ly α damping wing transmission of such a source is only $T = 15$ per cent, a factor of $> 5 \times$ lower than if the galaxy were to lie at the centre of a very large ($R > 3 \text{ physical Mpc}$) ionized bubble ($T \gtrsim 80$ per cent). If $\gtrsim 80$ per cent of Ly α photons emitted by faint galaxies in our targeted $z \simeq 6.8$ volume do in fact transmit through the IGM, we would expect to see a small evolution in the Ly α -emitter fraction from $z \sim 6$ (Castellano et al. 2018), in contrast to what is generally reported in the literature (e.g. Stark, Ellis & Ouchi 2011; Caruana et al. 2014; Schenker et al. 2014; Tilvi et al. 2014; De Barros et al. 2017; Pentericci et al. 2018).

Because the wide-area COSMOS field is currently only covered by ground-based near-infrared imaging, we cannot yet identify faint galaxies in our targeted $z \simeq 6.8$ volume for Ly α follow-up. However, upcoming *JWST* observations with the COSMOS-Webb program will partially cover this field (see Fig. 1) with 5σ depths of $m \approx 27.5$ – 28 in the NIRCcam F115W, F150W, F277W, and F444W filters (Kartaltepe et al. 2021). Adopting the $z \sim 7$ luminosity function from Bouwens et al. (2021b), we estimate that COSMOS-Webb observations will enable the detection of $\gtrsim 100$ $z = 6.7$ – 6.9 galaxies with $M_{\text{UV}} \leq -19$ ($m < 28$) within our targeted field assuming an overdensity of $N(N) \gtrsim 3$. Deep Ly α follow-up observations of these systems would clearly help distinguish whether our targeted region of COSMOS

contains many small-to-moderate sized ($R \sim 0.5\text{--}1$ physical Mpc) ionized bubbles or a single very large ($R \gtrsim 3$ physical Mpc) bubble.

5 SUMMARY AND OUTLOOK

In this work, we have sought to better characterize the size and associated overdensity of a tentative large ($R > 1$ physical Mpc) ionized bubble at $z \simeq 6.8$ we previously identified in E21b. To accomplish this goal, we conducted deep Ly α spectroscopy of 10 UV-bright ($M_{\text{UV}} \leq -20.4$) Lyman-break galaxies at $z \simeq 6.6\text{--}6.9$ surrounding this possible ionized bubble in an 11×15 arcmin² area. Below is a summary of our results and conclusions:

(i) We confidently detect ($S/N > 7$) Ly α emission in nine of 10 targeted galaxies, yielding redshifts spanning $z_{\text{Ly}\alpha} = 6.701\text{--}6.882$ consistent with our photometric selection window. The Ly α fluxes range between $(3.7\text{--}18.5) \times 10^{-18}$ erg s⁻¹ cm⁻² and line widths span FWHM $\approx 150\text{--}540$ km s⁻¹ with a median of 272 km s⁻¹.

(ii) We quantify the spectroscopic overdensity within the 140 physical Mpc³ volume spanned by our Ly α -detected sources. This volume contains at least $3.0_{-0.9}^{+9.0}$ times the number of $M_{\text{UV}} \leq -21$ systems expected on average from wide-area luminosity functions (Bowler et al. 2017; Harikane et al. 2021). Our spectra therefore confirm that this region of COSMOS traces a strong, large-scale galaxy overdensity at $z = 6.8$.

(iii) We estimate that each of our UV-bright ($M_{\text{UV}} \leq -20.4$) galaxies could potentially generate ionized bubbles with radii spanning $R = 0.69\text{--}1.13$ physical Mpc. These size estimates suggest that the three closely separated ($D = 0.2\text{--}1.8$ physical Mpc) galaxy pairs in our sample may each occupy a single ionized bubble due to overlap. If fainter ($M_{\text{UV}} \gtrsim -20$) galaxies contribute significantly to the ionizing photon budget, the entire overdense volume spanned by our confirmed Ly α emitters (characteristic radius $R = 3.2$ physical Mpc) may potentially be reionized. In this scenario, we would expect a typical Ly α damping wing transmission fraction of $T \approx 80$ per cent among our observed UV-bright galaxies. If these systems instead occupy more moderate-sized ($R \sim 1$ physical Mpc) bubbles, their Ly α IGM transmission fraction would be $\approx 2 \times$ lower ($T \approx 30\text{--}60$ per cent).

(iv) We test for enhanced Ly α emission among our sample to explore whether a very large ($R \sim 3$ physical Mpc) ionized bubble may exist within our targeted overdense volume. We detect strong Ly α emission ($\text{EW} > 25$ Å) from 40 per cent (4/10) of our observed UV-bright galaxies, a factor $\approx 4\text{--}5$ higher than that typically found among similarly luminous ($M_{\text{UV}} < -20.25$) $z \sim 7$ systems (Schenker et al. 2014; Pentericci et al. 2018). The median Ly α EW of our targeted sample (≥ 20 Å) is also enhanced by at least a factor of $2.0_{-0.5}^{+0.9}$ relative to that inferred from a larger ($N = 22$) sample of equally luminous $z \simeq 6.6\text{--}6.9$ galaxies ($\text{EW} = 10 \pm 3$ Å; E21b). We find no clear evidence of significant differences in the typical Ly α photon production or escape efficiency between our sample and that of E21b based on the inferred galaxy properties from SED fitting. The enhanced Ly α emission of our sample may instead indicate that the 140 physical Mpc³ volume hosting these systems is highly reionized, a scenario that is qualitatively consistent with expectations given the surrounding strong, large-scale galaxy overdensity (e.g. Barkana & Loeb 2004; Hutter et al. 2017; Qin et al. 2022).

(v) We investigate whether the Ly α profiles from our sample also support the presence of a surrounding very large ionized bubble (e.g. Matthee et al. 2018). One of our galaxies (COS-1009842; $z_{\text{Ly}\alpha} = 6.76$) displays a Ly α velocity profile that is indistinguishable from a symmetric Gaussian, potentially suggesting that the peak of this

line traces systemic velocity. If this scenario is confirmed, it would indicate that blue-sided Ly α photons emitted from COS-1009842 face very little optical depth from the surrounding IGM (as well as from the ISM and CGM), thereby necessitating a very large ($R \gtrsim 3$ physical Mpc) ionized bubble within our observed volume (Mason & Gronke 2020).

(vi) Ly α spectra of fainter ($M_{\text{UV}} > -20$) $z \simeq 6.8$ galaxies can further help characterize the IGM ionization state within our observed overdense field. Given the expected smaller velocity offsets of fainter sources (Erb et al. 2014; Stark et al. 2017; Mason et al. 2018), such galaxies may show up to a factor of ~ 5 increase in Ly α EW relative to average if they occupy a very large ($R > 3$ physical Mpc) ionized bubble. We estimate that the *JWST* COSMOS-Webb survey will detect $\gtrsim 100$ faint ($M_{\text{UV}} \leq -19$) $z = 6.7\text{--}6.9$ galaxies within our targeted field assuming an overdensity of $N/(N) \gtrsim 3$. Deep Ly α follow-up observations of these fainter systems would clearly help distinguish whether our targeted region of COSMOS contains many small-to-moderate sized ($R \sim 0.5\text{--}1$ physical Mpc) ionized bubbles or a single very large ($R \gtrsim 3$ physical Mpc) bubble.

This study demonstrates how wide-area $z \gtrsim 7$ Ly α spectroscopy can help identify and characterize large ionized bubbles formed during reionization. Upcoming facilities such as the Nancy Grace Roman Space Telescope as well as the Giant Magellan Telescope will enable the selection and spectroscopic follow-up of massive, UV-luminous $z \gtrsim 7$ galaxies across much wider areas (1000 deg²), allowing the opportunity to further study the largest H II regions present in the early Universe. Combining such studies with 21-cm observations from e.g. LOFAR, HERA, and SKA will deliver rich insight into how intergalactic H II regions formed and grew during reionization.

ACKNOWLEDGEMENTS

The authors sincerely thank the anonymous referee for their helpful, constructive comments. The authors also thank John Chisholm for insightful conversations that benefited this work, as well as Stéphane Charlot and Jacopo Chevallard for providing access to the BEAGLE SED fitting code. Both authors acknowledge funding from NASA *JWST*/NIRCam contract to the University of Arizona, NAS5-02015. DPS acknowledges support from the National Science Foundation through the grant AST-2109066.

Observations reported here were obtained at the MMT Observatory, a joint facility of the University of Arizona and the Smithsonian Institution. RE sincerely thanks the MMT queue observers Michael Calkins, Ryan Howie, ShiAnne Kattner, and Skyler Self for their assistance in collecting the Binospec data, as well as Ben Weiner for managing the queue. Based on data products from observations made with ESO Telescopes at the La Silla Paranal Observatory under ESO programme ID 179.A-2005 and on data products produced by CALET and the Cambridge Astronomy Survey Unit on behalf of the UltraVISTA consortium. This research has made use of the NASA/IPAC Infrared Science Archive, which is funded by the National Aeronautics and Space Administration (NASA) and operated by the California Institute of Technology. This work is based [in part] on observations made with the *Spitzer Space Telescope*, which was operated by the Jet Propulsion Laboratory, California Institute of Technology under a contract with NASA.

The Hyper Suprime-Cam (HSC) collaboration includes the astronomical communities of Japan and Taiwan, and Princeton University. The HSC instrumentation and software were developed by the National Astronomical Observatory of Japan (NAOJ), the Kavli

Institute for the Physics and Mathematics of the Universe (Kavli IPMU), the University of Tokyo, the High Energy Accelerator Research Organization (KEK), the Academia Sinica Institute for Astronomy and Astrophysics in Taiwan (ASIAA), and Princeton University. Funding was contributed by the FIRST program from the Japanese Cabinet Office, the Ministry of Education, Culture, Sports, Science and Technology (MEXT), the Japan Society for the Promotion of Science (JSPS), Japan Science and Technology Agency (JST), the Toray Science Foundation, NAOJ, Kavli IPMU, KEK, ASIAA, and Princeton University. This paper makes use of software developed for Vera C. Rubin Observatory. We thank the Rubin Observatory for making their code available as free software at <http://pipelines.lsst.io/>. This paper is based on data collected at the Subaru Telescope and retrieved from the HSC data archive system, which is operated by the Subaru Telescope and Astronomy Data Center (ADC) at NAOJ. Data analysis was in part carried out with the cooperation of Center for Computational Astrophysics (CfCA), NAOJ. We are honored and grateful for the opportunity of observing the Universe from Maunakea, which has the cultural, historical, and natural significance in Hawaii.

This research made use of ASTROPY, a community-developed core PYTHON package for Astronomy (Astropy Collaboration et al. 2013; Price-Whelan et al. 2018); MATPLOTLIB (Hunter 2007); NUMPY (Harris et al. 2020); and SCIPY (Virtanen et al. 2020).

DATA AVAILABILITY

The optical through mid-infrared imaging data underlying this article are available through their respective data repositories. See <https://hsc-release.mtk.nao.ac.jp/doc/> for HSCSSP data, <https://hsc-release.mtk.nao.ac.jp/doc/index.php/chorus/> for CHORUS data, <https://irsa.ipac.caltech.edu/data/COSMOS/> for HST F814W data, <http://www.eso.org/rm/publicAccess#/dataReleases> for UltraVISTA data, and <https://sha.ipac.caltech.edu/applications/Spitzer/SHA/> for IRAC data. The MMT/Binospec data will be shared upon reasonable request to the corresponding author.

REFERENCES

Aihara H. et al., 2018, *PASJ*, 70, S4
 Aihara H. et al., 2019, *PASJ*, 71, 114
 Ashby M. L. N. et al., 2018, *ApJ*, 237, 39
 Astropy Collaboration, 2013, *A&A*, 558, A33
 Barkana R., Loeb A., 2004, *ApJ*, 609, 474
 Begley R. et al., 2022, preprint (arXiv:2202.04088)
 Bouwens R. J. et al., 2014, *ApJ*, 793, 115
 Bouwens R. J. et al., 2021a, preprint (arXiv:2106.13719)
 Bouwens R. J. et al., 2021b, *AJ*, 162, 47
 Bowler R. A. A. et al., 2014, *MNRAS*, 440, 2810
 Bowler R. A. A., Dunlop J. S., McLure R. J., McLeod D. J., 2017, *MNRAS*, 466, 3612
 Bowler R. A. A., Jarvis M. J., Dunlop J. S., McLure R. J., McLeod D. J., Adams N. J., Milvang-Jensen B., McCracken H. J., 2020, *MNRAS*, 493, 2059
 Bruzual G., Charlot S., 2003, *MNRAS*, 344, 1000
 Caruana J., Bunker A. J., Wilkins S. M., Stanway E. R., Lorenzoni S., Jarvis M. J., Ebert H., 2014, *MNRAS*, 443, 2831
 Castellano M. et al., 2016, *ApJ*, 818, L3
 Castellano M. et al., 2018, *ApJ*, 863, L3
 Chabrier G., 2003, *PASP*, 115, 763
 Chevillard J., Charlot S., 2016, *MNRAS*, 462, 1415
 Chevillard J. et al., 2018, *MNRAS*, 479, 3264
 Ciardi B., Ferrara A., Governato F., Jenkins A., 2000, *MNRAS*, 314, 611
 Curtis-Lake E. et al., 2012, *MNRAS*, 422, 1425

Curtis-Lake E. et al., 2016, *MNRAS*, 457, 440
 Davies F. B. et al., 2018, *ApJ*, 864, 142
 De Barros S. et al., 2017, *A&A*, 608, A123
 De Barros S., Oesch P. A., Labbé I., Stefanon M., González V., Smit R., Bouwens R. J., Illingworth G. D., 2019, *MNRAS*, 489, 2355
 Du X., Shapley A. E., Tang M., Stark D. P., Martin C. L., Mobasher B., Topping M. W., Chevillard J., 2020, *ApJ*, 890, 65
 Endsley R., Stark D. P., Chevillard J., Charlot S., 2021a, *MNRAS*, 500, 5229 (E21a)
 Endsley R., Stark D. P., Charlot S., Chevillard J., Robertson B., Bouwens R. J., Stefanon M., 2021b, *MNRAS*, 502, 6044 (E21b)
 Endsley R. et al., 2022, preprint (arXiv:2202.01219)
 Erb D. K. et al., 2014, *ApJ*, 795, 33
 Fabricant D. et al., 2019, *PASP*, 131, 075004
 Ferland G. J. et al., 2013, *Rev. Mex. Astron. Astrofis.*, 49, 137
 Feroz F., Hobson M. P., 2008, *MNRAS*, 384, 449
 Feroz F., Hobson M. P., Bridges M., 2009, *MNRAS*, 398, 1601
 Finkelstein S. L. et al., 2012, *ApJ*, 756, 164
 Fletcher T. J., Tang M., Robertson B. E., Nakajima K., Ellis R. S., Stark D. P., Inoue A., 2019, *ApJ*, 878, 87
 Flury S. R. et al., 2022, preprint (arXiv:2201.11716)
 Fontana A. et al., 2010, *ApJ*, 725, L205
 Foreman-Mackey D., Hogg D. W., Lang D., Goodman J., 2013, *PASP*, 125, 306
 Fuller S. et al., 2020, *ApJ*, 896, 156
 Furlanetto S. R., Zaldarriaga M., Hernquist L., 2004, *ApJ*, 613, 1
 Furlanetto S. R., Zaldarriaga M., Hernquist L., 2006, *MNRAS*, 365, 1012
 Furusawa H. et al., 2016, *ApJ*, 822, 46
 Garaldi E., Kannan R., Smith A., Springel V., Pakmor R., Vogelsberger M., Hernquist L., 2022, *MNRAS*, preprint (arXiv:2110.01628)
 Gazagnes S., Chisholm J., Schaerer D., Verhamme A., Izotov Y., 2020, *A&A*, 639, A85
 Gronke M. et al., 2021, *MNRAS*, 508, 3697
 Gutkin J., Charlot S., Bruzual G., 2016, *MNRAS*, 462, 1757
 Haiman Z., 2002, *ApJ*, 576, L1
 Haiman Z., Loeb A., 1997, *ApJ*, 483, 21
 Harikane Y. et al., 2021, preprint (arXiv:2108.01090)
 Harris C. R. et al., 2020, *Nature*, 585, 357
 Hashimoto T. et al., 2019, *PASJ*, 71, 71
 Hathi N. P. et al., 2016, *A&A*, 588, A26
 Henry A., Scarlata C., Martin C. L., Erb D., 2015, *ApJ*, 809, 19
 Hoag A. et al., 2019, *ApJ*, 878, 12
 Horne K., 1986, *PASP*, 98, 609
 Hu E. M., Cowie L. L., Capak P., McMahon R. G., Hayashino T., Komiyama Y., 2004, *AJ*, 127, 563
 Hu W. et al., 2021, *Nat. Astron.*, 5, 485
 Hunter J. D., 2007, *Comput. Sci. Eng.*, 9, 90
 Hutter A., Dayal P., Müller V., Trott C. M., 2017, *ApJ*, 836, 176
 Iliev I. T., Mellema G., Pen U. L., Merz H., Shapiro P. R., Alvarez M. A., 2006, *MNRAS*, 369, 1625
 Inoue A. K. et al., 2020, *PASJ*, 72, 101
 Izotov Y. I., Schaerer D., Thuan T. X., Worseck G., Guseva N. G., Orlitová I., Verhamme A., 2016a, *MNRAS*, 461, 3683
 Izotov Y. I., Orlitová I., Schaerer D., Thuan T. X., Verhamme A., Guseva N. G., Worseck G., 2016b, *Nature*, 529, 178
 Izotov Y. I., Schaerer D., Worseck G., Guseva N. G., Thuan T. X., Verhamme A., Orlitová I., Fricke K. J., 2018a, *MNRAS*, 474, 4514
 Izotov Y. I., Worseck G., Schaerer D., Guseva N. G., Thuan T. X., Fricke Verhamme A., Orlitová I., 2018b, *MNRAS*, 478, 4851
 Jaskot A. E., Dowd T., Oey M. S., Scarlata C., McKinney J., 2019, *ApJ*, 885, 96
 Jensen H., Hayes M., Iliev I. T., Laursen P., Mellema G., Zackrisson E., 2014, *MNRAS*, 444, 2114
 Jung I. et al., 2017, *ApJ*, 834, 81
 Jung I. et al., 2020, *ApJ*, 904, 144
 Kannan R., Garaldi E., Smith A., Pakmor R., Springel V., Vogelsberger M., Hernquist L., 2022, *MNRAS*, 511, 4005
 Kinsky J. et al., 2019, *PASP*, 131, 075005

- Kartalpe J. et al., 2021, COSMOS-Webb: The Webb Cosmic Origins Survey, JWST Proposal. Cycle 1
- Koekemoer A. M. et al., 2007, *ApJS*, 172, 196
- Kornei K. A., Shapley A. E., Erb D. K., Steidel C. C., Reddy N. A., Pettini M., Bogosavljević M., 2010, *ApJ*, 711, 693
- Kriek M. et al., 2015, *ApJS*, 218, 15
- Kunth D., Mas-Hesse J. M., Terlevich E., Terlevich R., Lequeux J., Fall S. M., 1998, *A&A*, 334, 11
- Leonova E. et al., 2021, preprint ([arXiv:2112.07675](https://arxiv.org/abs/2112.07675))
- Lin Y., Oh S. P., Furlanetto S. R., Sutter P. M., 2016, *MNRAS*, 461, 3361
- McCracken H. J. et al., 2012, *A&A*, 544, A156
- McGreer I. D., Mesinger A., D'Odorico V., 2015, *MNRAS*, 447, 499
- McQuinn M., Hernquist L., Zaldarriaga M., Dutta S., 2007, *MNRAS*, 381, 75
- Maiolino R. et al., 2015, *MNRAS*, 452, 54
- Makovoz D., Khan I., 2005, in Shopbell P., Britton M., Ebert R., eds, ASP Conf. Ser. Vol. 347, Astronomical Data Analysis Software and Systems XIV. Astron. Soc. Pac., San Francisco, p. 81
- Mason C. A., Gronke M., 2020, *MNRAS*, 499, 1395
- Mason C. A., Treu T., Dijkstra M., Mesinger A., Trenti M., Pentericci L., de Barros S., Vanzella E., 2018, *ApJ*, 856, 2
- Mason C. A. et al., 2019, *MNRAS*, 485, 3947
- Massey R., Stoughton C., Leauthaud A., Rhodes J., Koekemoer A., Ellis R., Shaghoulain E., 2010, *MNRAS*, 401, 371
- Matthee J., Sobral D., Best P., Khostovan A. A., Oteo I., Bouwens R., Röttgering H., 2017, *MNRAS*, 465, 3637
- Matthee J., Sobral D., Gronke M., Paulino-Afonso A., Stefanon M., Röttgering H., 2018, *A&A*, 619, A136
- Mesinger A., Haiman Z., Cen R., 2004, *ApJ*, 613, 23
- Meyer R. A., Laporte N., Ellis R. S., Verhamme A., Garel T., 2021, *MNRAS*, 500, 558
- Miralda-Escudé J., 1998, *ApJ*, 501, 15
- Miralda-Escudé J., Haehnelt M., Rees M. J., 2000, *ApJ*, 530, 1
- Naidu R. P. et al., 2022, *MNRAS*, 510, 4582
- Oke J. B., Gunn J. E., 1983, *ApJ*, 266, 713
- Ono Y. et al., 2012, *ApJ*, 744, 83
- Osterbrock D. E., Ferland G. J., 2006, *Astrophysics of Gaseous Nebulae and Active Galactic Nuclei*, University Science Books, Sausalito, CA, USA
- Pahl A. J., Shapley A., Steidel C. C., Chen Y., Reddy N. A., 2021, *MNRAS*, 505, 2447
- Park H. et al., 2021, *ApJ*, 922, 263
- Pei Y. C., 1992, *ApJ*, 395, 130
- Pentericci L., Grazian A., Fontana A., Castellano M., Giallongo E., Salimbeni S., Santini P., 2009, *A&A*, 494, 553
- Pentericci L. et al., 2014, *ApJ*, 793, 113
- Pentericci L. et al., 2016, *ApJ*, 829, L11
- Pentericci L. et al., 2018, *A&A*, 619, A147
- Price-Whelan A. M. et al., 2018, *AJ*, 156, 123
- Qin Y., Wyithe J. S. B., Oesch P. A., Illingworth G. D., Leonova E., Mutch S. J., Naidu R. P., 2022, *MNRAS*, 510, 3858
- Robertson B. E., 2021, preprint ([arXiv:2110.13160](https://arxiv.org/abs/2110.13160))
- Robertson B. E. et al., 2013, *ApJ*, 768, 71
- Rodríguez Espinosa J. M., Mas-Hesse J. M., Calvi R., 2021, *MNRAS*, 503, 4242
- Saxena A. et al., 2022, *MNRAS*, 511, 120
- Schenker M. A., Ellis R. S., Konidaris N. P., Stark D. P., 2014, *ApJ*, 795, 20
- Shapley A. E., Steidel C. C., Pettini M., Adelberger K. L., 2003, *ApJ*, 588, 65
- Shapley A. E., Steidel C. C., Strom A. L., Bogosavljević M., Reddy N. A., Siana B., Mostardi R. E., Rudie G. C., 2016, *ApJ*, 826, L24
- Shibuya T., Ouchi M., Harikane Y., 2015, *ApJS*, 219, 15
- Shivaei I. et al., 2018, *ApJ*, 855, 42
- Smit R. et al., 2014, *ApJ*, 784, 58
- Smit R. et al., 2015, *ApJ*, 801, 122
- Smith A., Kannan R., Garaldi E., Vogelsberger M., Pakmor R., Springel V., Hernquist L., 2021, preprint ([arXiv:2110.02966](https://arxiv.org/abs/2110.02966))
- Stark D. P., Ellis R. S., Chiu K., Ouchi M., Bunker A., 2010, *MNRAS*, 408, 1628
- Stark D. P., Ellis R. S., Ouchi M., 2011, *ApJ*, 728, L2
- Stark D. P. et al., 2017, *MNRAS*, 464, 469
- Stefanon M. et al., 2019, *ApJ*, 883, 99
- Steidel C. C., Erb D. K., Shapley A. E., Pettini M., Reddy N., Bogosavljević M., Rudie G. C., Rakic O., 2010, *ApJ*, 717, 289
- Steidel C. C., Bogosavljević M., Shapley A. E., Reddy N. A., Rudie G. C., Pettini M., Trainor R. F., Strom A. L., 2018, *ApJ*, 869, 123
- Steinhardt C. L. et al., 2014, *ApJ*, 791, L25
- Szalay A. S., Connolly A. J., Szokoly G. P., 1999, *AJ*, 117, 68
- Tang M., Stark D. P., Chevallard J., Charlot S., 2019, *MNRAS*, 489, 2572
- Tang M., Stark D. P., Chevallard J., Charlot S., Endsley R., Congiu E., 2021, *MNRAS*, 503, 4105
- Tang M., Stark D. P., Ellis R. S., 2022, preprint ([arXiv:2202.04142](https://arxiv.org/abs/2202.04142))
- Tilvi V. et al., 2014, *ApJ*, 794, 5
- Tilvi V. et al., 2020, *ApJ*, 891, L10
- Trainor R. F., Strom A. L., Steidel C. C., Rudie G. C., 2016, *ApJ*, 832, 171
- Vanzella E. et al., 2018, *MNRAS*, 476, L15
- Virtanen P. et al., 2020, *Nat. Methods*, 17, 261
- Wang F. et al., 2020, *ApJ*, 896, 23
- Weinberger L. H., Kulkarni G., Haehnelt M. G., Choudhury T. R., Puchwein E., 2018, *MNRAS*, 479, 2564
- Whitler L. R., Mason C. A., Ren K., Dijkstra M., Mesinger A., Pentericci L., Trenti M., Treu T., 2020, *MNRAS*, 495, 3602
- Willott C. J., Carilli C. L., Wagg J., Wang R., 2015, *ApJ*, 807, 180
- Wyithe J. S. B., Loeb A., 2005, *ApJ*, 625, 1
- Yang J. et al., 2020, *ApJ*, 897, L14

This paper has been typeset from a $\text{\TeX}/\text{\LaTeX}$ file prepared by the author.